

Supporting information

Black Gold Layers: Preparation via Thermal Evaporation, Material and Optical Properties, Application Potential for Gas Sensors

Jan Kejzlar,^{*a,b} Joris More-Chevalier,^{a,b} Martin Hruška,^a Jaroslav Otta,^a Přemysl Fitl,^a Michal Novotný,^{a,b} Morgane Poupon,^b Petr Hruška,^{b,c} Dejan Prokop,^c Stanislav Cichoň,^b Ladislav Fekete,^b Veronica Goian,^b Stanislav Kamba,^b Jakub Čížek,^c Maik Butterling,^d Maciej Oskar Liedke,^d Eric Hirschmann,^d Andreas Wagner,^d Martin Vrnáta^a and Ján Lančok^b

^a University of Chemistry and Technology, Technická 5, 16628 Prague 6, Czech Republic.

^b Institute of Physics of the Czech Academy of Sciences, Na Slovance 1999/2, 18200 Prague 8, Czech Republic.

^c Charles University, Faculty of Mathematics and Physics, V Holešovičkách 747/2, 18000 Prague 8, Czech Republic.

^d Institute of Radiation Physics, Helmholtz-Zentrum Dresden-Rossendorf, Bautzner Landstraße 400, 01328 Dresden, Germany

Table of contents

S1 XPS analysis of the individual chemical components of the deposited films

S2 SNR calculation details

S3 Particle size distribution analysis

S4 FFT analysis of the AFM topography

S5 Contact angle measurements data

Figures:

Fig.S1: Detail XPS analysis for reflective (A) and black (B) gold.

Fig.S2: SNR illustration & comparison.

Fig.S3: Particle size distribution of the black gold film.

Fig.S4.1: FFT analysis of the AFM images. Reflective gold with an FOV of 5 μm (A) and 20 μm (B). Black gold with an FOV of 5 μm (C) and 20 μm (D).

Fig.S4.2: 2D autocorrelation of the FFT images presented in the Figure 2. Reflective gold with an FOV of 5 μm (A) and 20 μm (B). Black gold with an FOV of 5 μm (C) and 20 μm (D).

Equations:

Eqn.ES1: Calculation of the *signal-to-noise* ratio.

Tables:

Table TS1: Data from the contact angle measurements.

S1 XPS analysis of the individual chemical components of the deposited films

Regarding the reference reflective gold sample, as presented in Figure S1-A, Au 4f peak is well fitted with a slightly asymmetric doublet. The Binding Energy position, Au 4f $^{7/2}$ at 84.0 eV, peak shape and doublet splitting, 3.68 eV, perfectly agree with the reference for a pure metallic gold¹. The 84.0 eV position also implies that most probably no charging was present during measurements and so no charge correction was necessary.

W 4f peak is found at 35.9 eV which matches to positions reported for WO₃ (35.9 eV)². Hence, we assume the tungsten chemistry to be WO₃.

Further, C 1s peak position and shape are typical for the adventitious carbon contamination (AdC)¹. The AdC is common for air exposed surfaces. There is a main peak component at 284.7 eV and a smaller higher binding energy shoulder at 285.9 eV. The first peak component corresponds to carbon – carbon bonds and carbon – hydrogen bonds while the second one to carbon – oxygen bonds.

The last spectrum presented is focused on O 1s region. Here, we can identify two peak components. We ascribe the lower one (531.2 eV) to the WO₃ mentioned above and the higher one (532.6 eV) to carbon – oxygen bonds of the AdC. However, we note that bonding assignment based on O 1s is less precise as it is difficult to find a unique Binding Energy position for a given chemical specie².

Regarding the black gold sample surface (Figure S1-B) and its comparison with the reference reflective gold sample surface, it can be stated that all respective XPS spectra are highly comparable. Consequently, there are practically no differences in chemistry between both surfaces. Only the Au 4f $^{7/2}$ peak of black gold is found at 84.1 eV but this falls within the measurement error + / - 0.2 eV.

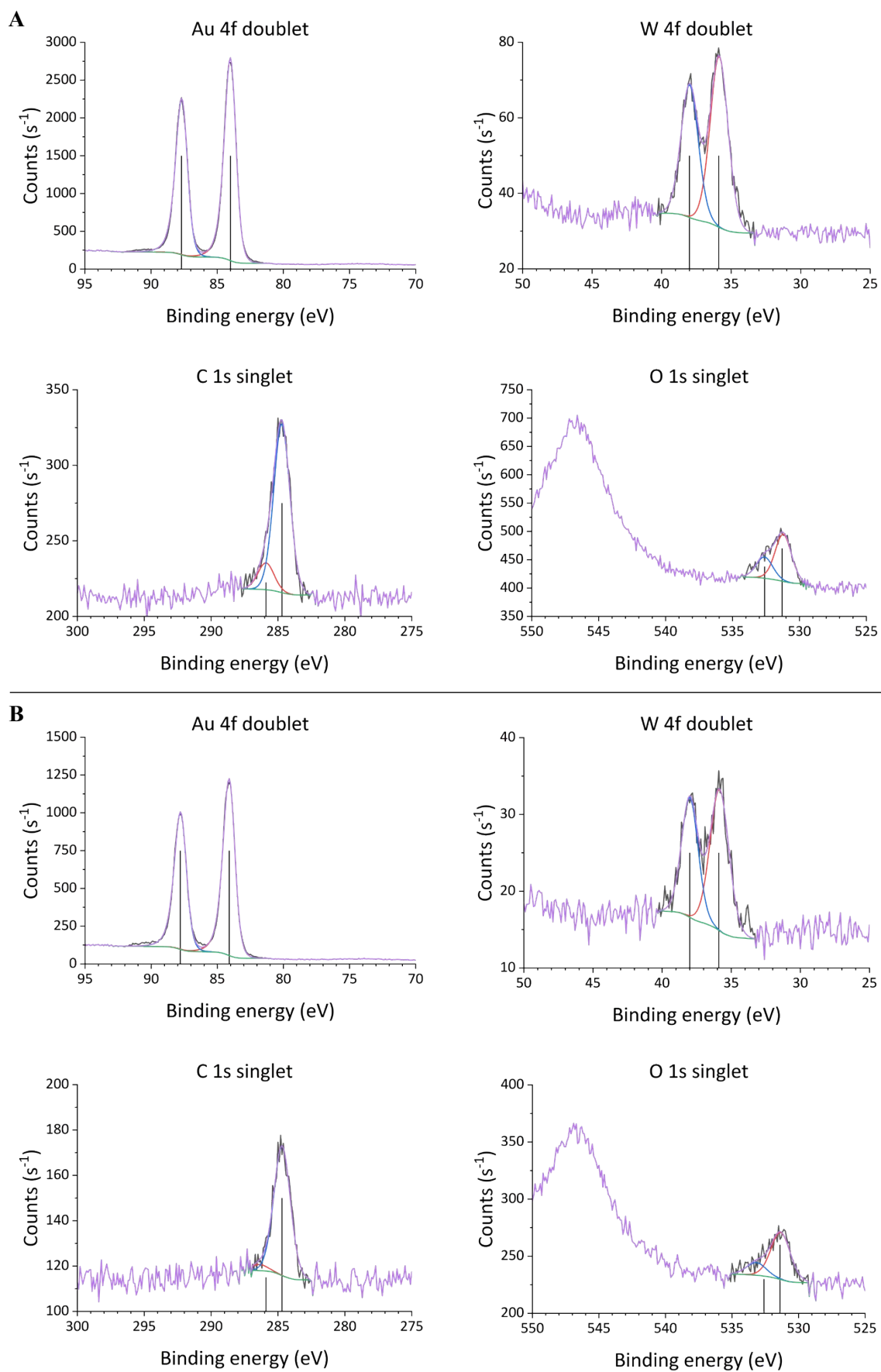


Figure S1: Detail XPS analysis for reflective (A) and black (B) gold.

S2 SNR calculation details

The method for calculating SNR was adopted from^{3,4}. In our case, the output signal is the sensor response (Y) divided by normalised noise level (Y_{Noise}) defined by the Eqn. ES1.

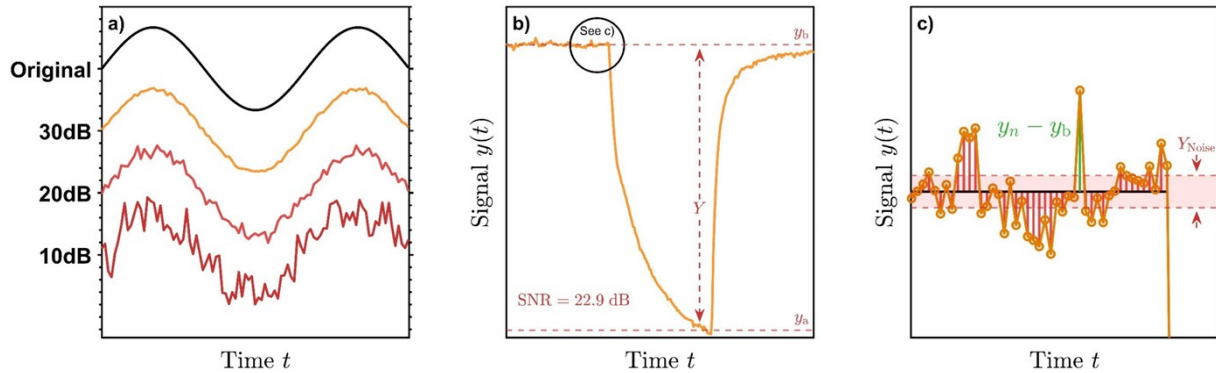


Figure S2: SNR illustration & comparison: a) Comparison of sinusoidal signal with different SNR; b) graphical illustration for the SNR evaluation in the usual sensor signal; c) detail of baseline signal and graphical illustration of the Y_{Noise} calculation⁵.

$$SNR = \frac{Y}{Y_{Noise}} = \frac{\Delta y}{\sqrt{\frac{1}{N} \sum_{n=1}^N (y_n - y_b)^2}}$$

(Eqn.

ES1)

S3 Particle size distribution analysis

The samples of black gold were measured using ImageJ software to assess their size. Total of 250 particles were measured for both top-down and cross-section measurements. The particles were approximated as a ball with a circular cut. The results can be seen in Fig.1. We can observe a rising trend in number of particles with decreasing diameter, only exception to this rule are particles with the diameter of 30–40 nm. Also, for particles with the diameter of 10 nm and less, we were limited by the resolution of our electron microscope. It can be assumed that the number of particles with a diameter <10 nm is much higher, however it cannot be correctly measured using our equipment.

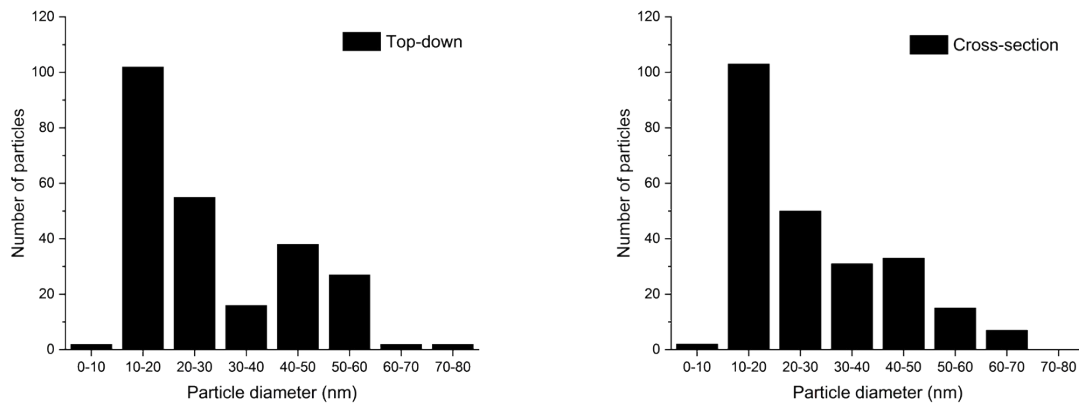


Figure S3: Particle size distribution of the black gold film.

S4 FFT analysis of the AFM topography

The FFT analysis was done to check the gold structures for any sort of repeating pattern in the sample's morphology. In the FFT images, there is no evidence of the periodic assembly of the grains. The grains are randomly distributed. The slightly visible line structure in the center of the S4.1-B image corresponds to the large lines-features visible on the substrate in the original image of the surface. Neither the 2D autocorrelation (Fig.S4.2) shows any significant features but the image of the autocorrelation of the average grain in the center of the images.

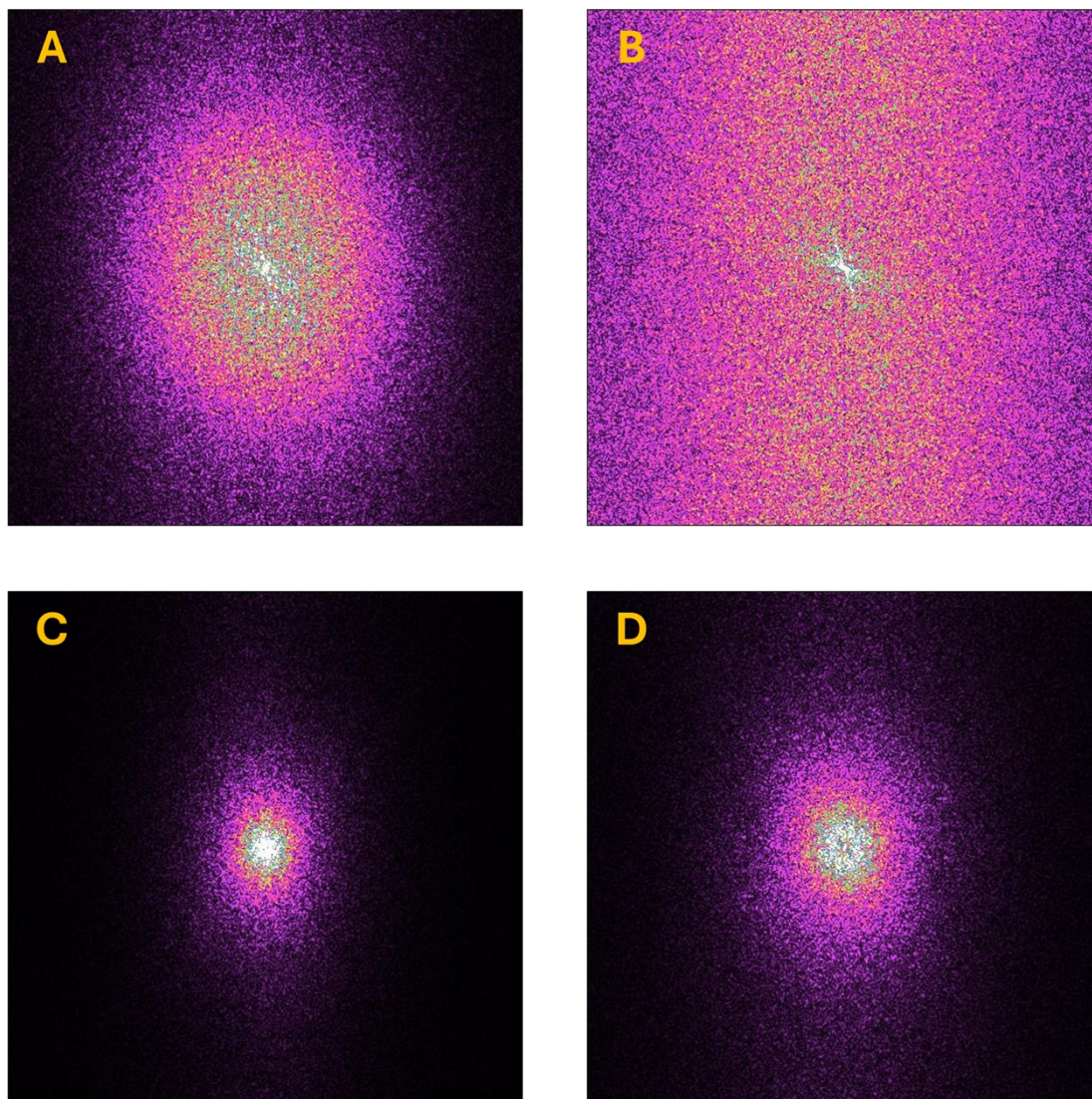


Figure S4.1: FFT analysis of the AFM images. Reflective gold with an FOV of 5 μm (A) and 20 μm (B). Black gold with an FOV of 5 μm (C) and 20 μm (D).

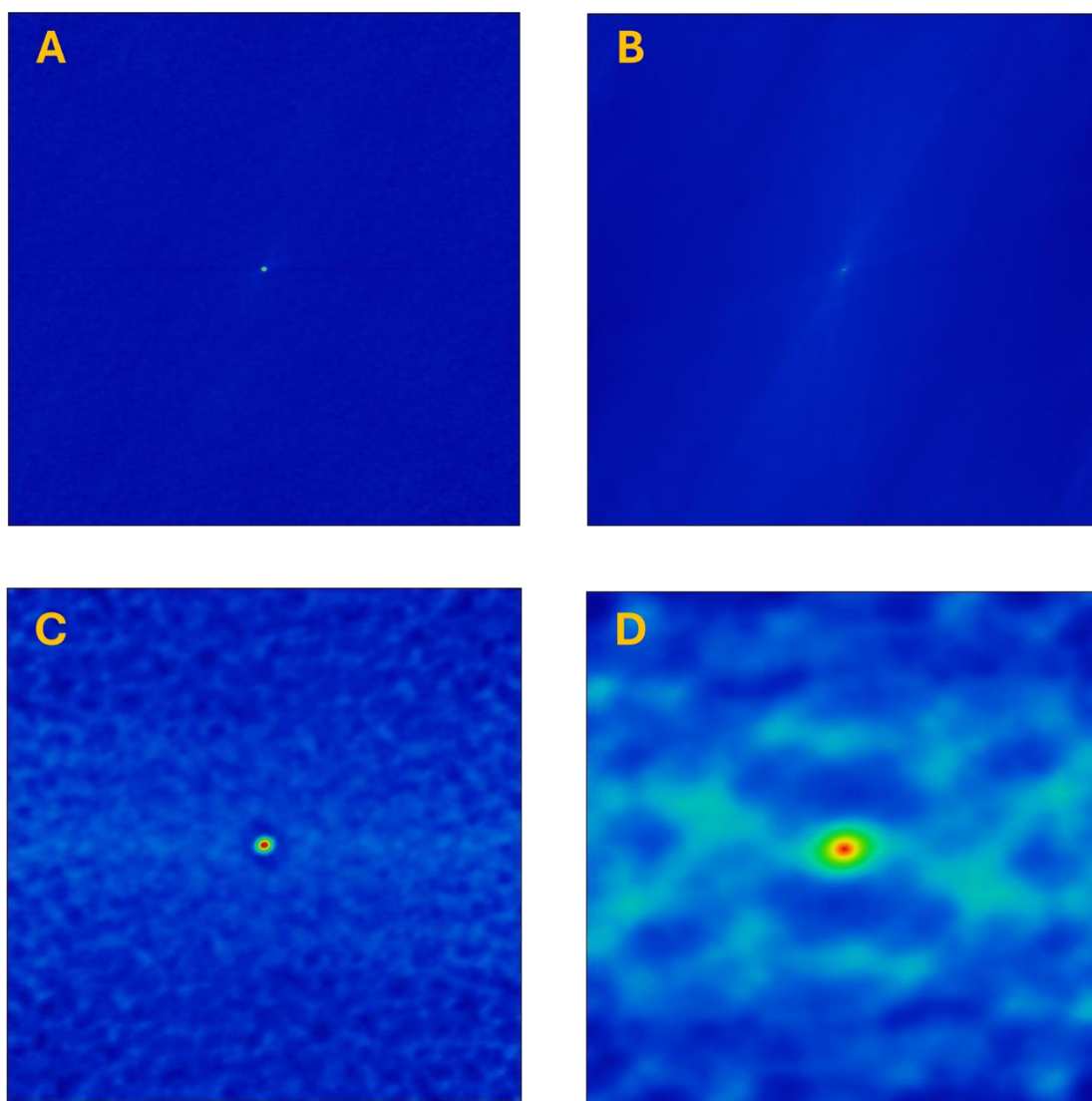


Figure S4.2: 2D autocorrelation of the FFT images presented in the Figure 2. Reflective gold with an FOV of 5 μm (A) and 20 μm (B). Black gold with an FOV of 5 μm (C) and 20 μm (D).

S5 Contact angle measurements data

The contact angle measurements were performed on both reflective and black gold samples. As one can see in table TS1, the interfacial tension for the reflective gold changes dramatically with each measurement, rendering the accurate determination impossible.

Table TS1: Data from the contact angle measurements.

Reflective Gold		Black Gold	
Theta [°]	Interfacial Tension [mN/m]	Theta [°]	Interfacial Tension [mN/m]
62.4	77.36	137.6	11.19
64.5	7.27	140.7	10.85
60.3	23.75	139.6	10.22
66.4	17.62	141.2	11.31
72.9	4.41	139.7	10.24
		139.5	10.29

References

- 1 XPS database, xpsdatabase.net.
- 2 XPS fitting, www.xpsfitting.com.
- 3 K. Chikkadi, M. Muoth, W. Liu, V. Maiwald and C. Hierold, *Sensors Actuators, B Chem.*, 2014, **196**, 682–690.
- 4 D. Kumar, P. Chaturvedi, P. Saho, P. Jha, A. Chouksey, M. Lal, J. S. B. S. Rawat, R. P. Tandon and P. K. Chaudhury, *Sensors Actuators, B Chem.*, 2017, **240**, 1134–1140.
- 5 M. Hruška, University of Chemistry and Technology, 2024.